Photo–Fenton reaction in the presence of morphologically controlled hematite as iron source

UNIVERSITÀ DEGLI STUDI DI TORINO

Photo-Fenton reaction in the presence of morphologically controlled hematite as iron source

Luca Demarchis, Marco Minella, Roberto Nisticò, Valter Maurino, Claudio Minero, Davide Vione*

Università di Torino, Dipartimento di Chimica, Via Pietro Giuria 5-7, 10125 Torino, Italy.

* Corresponding Author

E-mail: *davide.vione@unito.it*. Phone +39-011-6705296. Fax: +39-011-6705242.

Abstract

Hematite particles with controlled size and shape (cubic, spherical and ovoidal, with size range from hundreds nm to μm) were produced by modulating the conditions of synthesis and were characterized by different techniques (XRD spectroscopy, scanning electron microscopy, BET analysis, dynamic light scattering, UV-vis spectroscopy). The photoactivity of the synthesized hematite particles was tested towards the degradation of phenol under photo-Fenton conditions, obtaining optimal results in the pH range 3-4. Although the smaller particles have a larger contact interface between the solid and the solution, no obvious relationship was found between size and photoactivity. A possible explanation is that the smallest particles tested showed an important radiation scattering, which would interfere with radiation absorption and, therefore, with photoactivity. In contrast, the most photoactive samples were those showing the highest concentrations of leached iron. This issue would imply that photoactivity may be related to partial dissolution of hematite with formation of Fe(II) and of photo-active Fe(III) species, which activate the classic photo-Fenton process. Anyway, leached Fe was limited to the μg L^{-1} range that is safely far from the mg L^{-1} limits for wastewater.

Keywords: Hematite colloids; Photo-Fenton reaction; Advanced oxidation processes; Shape and size control.

1. Introduction

A major problem of emerging concern in the field of water quality is represented by the contamination of surface- and ground-waters with pollutants that are hardly removed by the traditional wastewater treatment plants (WWTPs) [1]. Therefore, WWTPs are increasingly regarded as potential emission sources for a wide range of substances such as pharmaceuticals and personal care products, flame retardants, artificial sweeteners and several industrial chemicals [2-4]. These compounds are often harmful to aquatic organisms because of toxicity, endocrine disruption properties and/or longer term effects, and they might also pose a threat to human health *via* their possible occurrence in drinking water [5-8]. To avoid such adverse effects, an important priority is represented by the technological update of WWTPs, so that they are enabled to remove recalcitrant pollutants [9,10]. Among possible solutions, Advanced Oxidation Processes (AOPs) are increasingly regarded as a viable option because of their ability to decontaminate water from compounds that are difficult to be treated by other techniques [11-13]. Such processes are based on the formation of reactive transient species (including most notably, but not exclusively, the hydroxyl radical, $^{\bullet}OH$), which show remarkable reactivity toward a wide range of refractory pollutants [14,15].

Heterogeneous photo-Fenton systems are gaining increasing importance as AOPs in the field of wastewater treatment [16,17]. They consist in the use of solid Fe species under irradiation, in the presence of H_2O_2. A general scheme of the process can be outlined as follows [18,19]:

$$Fe^{III}\text{-}OH_{(s)} + h\nu \rightarrow Fe^{2+}_{(aq)} + {}^{\bullet}OH \quad (1)$$

$$Fe^{2+}_{(aq)} + H_2O_2 \rightarrow [Fe(III) + OH^{-}] \ (e.g.\ Fe^{III}\text{-}OH_{(s)}) + {}^{\bullet}OH \quad (2)$$

Depending on pH, the Fe(III) produced in reaction (2) may be dissolved, may form solid species or may precipitate on the surface of the existing oxide. In the latter cases, $Fe^{III}\text{-}OH_{(s)}$ represents a hydroxylated form of solid Fe(III) that would occur at the interface with water [17,18]. The generation of $^{\bullet}OH$ in reaction (2) is unlikely to be quantitative and it is pH-dependent, because iron super-oxidized species (such as the ferryl ion, FeO^{2+}) are also competitively formed as transients [20-22]. The heterogeneous photo-Fenton reaction combines several advantages that are extremely useful in the context of pollutant degradation [23-26]. The first advantage is the use of iron in the form of a solid catalyst, which is easily removed from the reaction system at the end of the treatment and can be recycled. In contrast, the removal of dissolved iron species to respect the Fe discharge limits in homogeneous processes usually requires a precipitation step that yields solid $Fe(OH)_3$. The latter is hardly recycled, because it is very different from the photoactive compounds that were initially used. Another positive issue is the possibility to activate the process with sunlight [27].

Among the solid Fe species that can be used in photo-Fenton systems, hematite (α-Fe_2O_3) is a reasonable choice because of its significant photoactivity, promoted by the photoreduction of

surface Fe^{III} species to Fe^{2+}, sometimes in the presence of complexing and/or reducing agents [28-31]. Moreover, α-Fe_2O_3 is easily synthesized by low-cost techniques [32,33]. A very interesting feature is the possibility to finely tune the size and shape of hematite particles, thereby obtaining α-Fe_2O_3 specimens with peculiar morphological properties [34]. With the aim to optimize the hematite photoactivity toward the heterogeneous photo-Fenton reaction, in the present work we assessed the ability of α-Fe_2O_3 samples, with different morphology and particle size, to degrade phenol as model compound under irradiation in the presence of H_2O_2. The structural and morphological properties of the synthesized hematites and the amount of photo-leached iron were compared with the photoactivity of the samples. The choice of phenol as substrate was motivated by various reasons. The first is that this compound has a well-known behavior under oxidative conditions [35], which makes its degradation very suitable to test the performance of newly synthesized photocatalysts. The second issue is that phenol is a widespread environmental pollutant. It is an important component of oil refinery wastes and it is also produced upon conversion of coal into gaseous or liquid fuels and during the manufacturing of metallurgical coke from coal. Its possible environmental sources include discharges of oil refineries, coal conversion plants, municipal waste treatment plants, or spills. Phenol is highly toxic to both humans and animals, and it is often incompletely removed by traditional treatment methods including physico-chemical and biological ones [36,37]. Therefore, it is important to investigate on techniques that are able to achieve its complete removal.

2. Experimental

2.1. Materials

Iron(III) chloride hexahydrate (> 99%), sodium hydroxide (> 99%), $NaNO_3$ (> 99%), perchloric acid (70%), hydrogen peroxide (35%), phenol (>99%), 1,4-benzoquinone (98%), sulfuric acid (95-97%) and methanol (>99.9%) were purchased from Sigma-Aldrich; Fe(III) perchlorate hydrate (99%) and Fe(III) nitrate nonahydrate (98%) were purchased from Alfa Aesar; iron(II) chloride tetrahydrate (> 99%), nitrilotriacetic acid trisodium salt (> 98%) and NH_3 were from Fluka; hydrochloric acid (37%), sodium chloride (> 99.5%), catechol (99%), resorcinol (99.5%) and ammonium thiocyanate (>99%) from Carlo Erba; hydroquinone (99%) and potassium persulfate (>98%) from Merck. Ultra-pure water was obtained with a Milli-Q^{TM} system (Millipore).

2.2. Hematite synthesis

Six samples of monodisperse hematite particles with different size and shape were obtained by following three different procedures, all involving modifications at key steps of the synthesis methods from the literature.

The first procedure is a modification of the synthesis proposed by Sugimoto et al. [38] and it allows the production of large quantities of hematite particles through a two-step phase

transformation, from a highly condensed $Fe(OH)_3$ gel to α-Fe_2O_3 *via* β-FeOOH (akaganeite) [39,40]. This is a gel-sol procedure, which differs from the usual sol-gel techniques because the conversion occurs from an initial dense gel of hydroxide to a final sol of hematite. First, 45 mL of NaOH (6 M) were added drop-wise to 50 mL of a well-stirred $FeCl_3 \cdot 6\ H_2O$ solution (2 M) in a Pyrex bottle. The gel was maintained under stirring for additional 10 minutes, and then heated at 100°C for 6 hours. This time allows for the conversion of $Fe(OH)_3$ into β-FeOOH. Later, the supernatant liquid was removed by centrifugation and the resulting β-FeOOH was washed twice with 0.5 M $NaNO_3$. The akaganeite precipitate was dispersed again in ultra-pure water by ultrasonication, to obtain 200 mL of stock suspension. To produce the hematite particles, well-stirred aliquots (20 mL) of the β-FeOOH stock suspension were added with 1.2 mL of HCl (1 M) and 8.8 mL of water. The final suspensions were stirred for 10 minutes and, afterwards, they were transferred in tightly closed bottles and heated at 100°C to allow conversion into hematite. This procedure allows for the synthesis of large hematite particles (diameter over 1 μm) with different morphologies, which can be obtained by using shape-control additives. Several anions have been reported to induce the anisotropic growth of hematite particles [39,40]. Anions can be selectively adsorbed at the surface of the nuclei and they can regulate the growth of specific crystal faces, thus determining the final particle morphology. The addition of anions such as chloride and nitrilotriacetate to the akaganeite suspensions was carried out before the final heat treatment. These modifications of the procedure allowed for the synthesis of pseudocubic (by adding chloride) and spherical hematite (with addition of nitrilotriacetate).

The second synthesis is a gel-sol procedure similar to the previous one, without the step of akaganeite washing [39,40]. First, 45 mL of NaOH (6 M) were slowly added to 50 mL of magnetically stirred $FeCl_3$ solution (2 M). The system thus obtained was kept under stirring for additional 10 minutes. The obtained $Fe(OH)_3$ gel was transferred into a tightly stoppered bottle and oven-heated at 100°C for at least 3 days to allow conversion into hematite. The shape control was obtained by adding chloride or nitrilotriacetate to the $Fe(OH)_3$ gel, as described above. The size control was obtained by varying the temperature of the $FeCl_3$ solution when NaOH was added. The nucleation rate is influenced by temperature, because a higher temperature causes the formation of a higher amount of nuclei and, subsequently, yields smaller particles. The temperature variation (25-90°C) allowed the synthesis of particles with diameters in the 300-1200 nm range (see Figure SM1a in the Supplementary Material, hereafter SM; *vide infra* for the determination of particle diameters).

The third method uses the catalytic phase-transformation mechanism proposed by Liu and co-workers [41], which enables lower conversion times by adding trace Fe^{II} to the initial $Fe(OH)_3$ gel. The standard experimental conditions for this procedure were as follows: NaOH (6 M) was slowly added to 50 mL of a magnetically stirred $FeCl_3$ solution (2 M unless otherwise reported) till pH 7 (measured with a Metrohm 691 pH meter, equipped with a Metrohm 6.0233.100 combined glass electrode). Then, $FeCl_2$ was added to the gel to have a ratio $[Fe^{II}]/[Fe^{III}] = 0.02$, and pH was readjusted to 7 by adding dilute NaOH. The system was kept under stirring for additional 10 minutes and then refluxed for at least 30 min until conversion occurred. This procedure yielded

spherical particles with diameters in the 100-400 nm range. The size control was obtained by varying the $FeCl_3$ concentration, with particle diameters increasing as concentration increased (see Figure SM1b in the SM).

All the prepared hematite samples underwent a final washing with ultra-pure water (three times), 1 M NH_3 (one time) and again with ultra-pure water (three times). Finally, all samples were dried at 70°C.

2.3. Physico-chemical characterization of hematite

The size and shape of the synthesized hematite particles were determined by scanning electron microscopy, with a Phenom Pro instrument operating at 5, 10 and 15 kV, 50.0 μA beam current and 50 pA probe intensity.

The particle hydrodynamic radii were determined by Dynamic Light Scattering (DLS). The used instrument was an ALV-NIBS High Performance Particle Sizer (ALV GmbH, Germany) equipped with a Ne-He laser and with an ALV-500 multiple tau digital correlator. Samples were suspended in ultra-pure water, and analyzed by recording the intensity of the scattered light at an angle of 173° for 30 seconds at 25°C. Suspensions with different hematite loadings were analyzed, and the results were extrapolated at infinite dilution.

The sample crystalline phases were determined by X-Ray Diffraction (XRD). XRD patterns were recorded with a PW3050/60 X'Pert PRO MPD diffractometer (PANalytical) working in Bragg-Brentano configuration. The X-ray source was a high-power ceramic tube (PW3373/10 LFF) with a Cu anode. The instrument was equipped with a Ni filter to attenuate Kb. Diffracted photons were collected by a real-time multiple strip X'celerator detector. Powder samples were hosted on an amorphous SiO_2 sample holder.

The specific surface area of the samples was determined by N_2 adsorption-desorption experiments. Analyses were carried out by means of an ASAP 2020 instrument (Micromeritics), which measures both the specific surface area (BET model, [42]) and the porosity (DFT model, [43,44]) of mesoporous samples. The Density Functional Theory (DFT) was applied to the simultaneous examination of the micro-, meso- and macroporosity of the samples (pores slit with low regularization). The analyses were performed on powders (*ca*. 0.7-1.0 g sample weight) that were outgassed for several hours at 30 °C *in vacuo* (the residual pressure was 10^{-2} mbar), to ensure complete removal of atmospheric contaminants from both surface and pores.

2.4. Photo-Fenton experiments

Photo-Fenton experiments were carried out in magnetically stirred Pyrex beakers, initially containing a stock hematite suspension. Milli-Q water, phenol, H_2O_2 and $HClO_4$ were added to achieve a volume of 50 mL and concentrations/loadings of 0.1 mM (phenol), 1.0 mM (H_2O_2) and 200 mg L^{-1} (α-Fe_2O_3), as well as to fix initial pH to the target value ($HClO_4$). Irradiation was carried out under a Philips TL09N lamp, with maximum emission at 355 nm and an irradiance of 18 W m^{-2} in the 295-400 nm range, measured with a CO.FO.ME.GRA. (Milan, Italy) power meter.

Dark runs were carried out by placing, under the same lamp, beakers wrapped with aluminum foil, to achieve comparable temperature and stirring conditions as for the irradiation experiments.

Each sample was irradiated for up to 4 hours and, every 30 minutes, 1.5 mL suspension aliquots were withdrawn and immediately filtered on hydrophilic PTFE Millex-LCR filters (0.45 μm pore diameter). A 0.7 mL volume of the filtered solution was put into a vial, containing 0.7 mL methanol to quench the Fenton reaction [27].

The concentrations of phenol and its intermediates were measured by High-Performance Liquid Chromatography coupled to Diode Array Detection (HPLC-DAD). The instrument used was a VWR Hitachi Elite chromatograph, equipped with L-2200 Autosampler (injection volume 60 μL), L-2130 quaternary pump for low-pressure gradients, L-2300 column oven (set at 40°C), and L-2455 DAD detector. The column used was a RP-C18 LichroCART (VWR Int., length 125 mm, diameter 4 mm), packed with LiChrospher 100 RP-18 (5 μm diameter). Elution was carried out with a 10:90 mixture of methanol: aqueous H_3PO_4 (pH 2.8) at 1.0 mL min^{-1} flow rate, with detection at 220 nm. The retention times were 16.1 min for phenol, and 3.4, 5.8, 6.4 and 7.3 min for hydroquinone, resorcinol, 1,4-benzoquinone and catechol, respectively. The column dead time was 0.9 min.

The determination of Fe released in solution was evaluated by a spectrophotometric procedure. A 1.5 mL aliquot of hematite suspension was withdrawn every 60 minutes of irradiation and filtered on hydrophilic PTFE Millex-LCR filters (0.45 μm pore diameter). Total iron was determined by oxidizing any Fe(II) to Fe(III) with persulfate (4 mg/L) and by complexing Fe(III) with thiocyanate (50 mg/L) in acidic conditions (1.25 M sulfuric acid). The absorption of the iron-thiocyanate complex was determined at 474 nm. Fe^{III} was determined in the same way, without the oxidative step, and Fe^{II} was obtained as the difference between total iron and Fe^{III} [45]. Spectrophotometric analyses were performed using a Varian CARY 100 Scan double-beam UV-Vis spectrophotometer, using quartz cuvettes with 10 cm path length. The detection limit of the technique was ~3 μg Fe L^{-1}, the quantification limit was ~10 μg Fe L^{-1}. The same spectrophotometric technique, with quartz cuvettes having an optical path length of 10 mm, was used to determine the exact Fe^{III} content in $Fe(ClO_4)_3$ hydrate, using $Fe(NO_3)_3 \cdot 9\ H_2O$ as reference compound.

The same UV-vis spectrophotometer, with 10 mm cuvettes, was used to measure the extinction spectra (absorption + scattering) of the studied hematite samples at a loading of 100 mg L^{-1} α-Fe_2O_3.

3. Results and discussion

3.1. Hematite characterization

Six hematite samples with different size and shape were prepared and tested. Three of the samples (C1, C2, C3) had cubic morphology, while the other three were either spherical (S1, S2) or ovoidal (O1). Table 1 reports the hydrodynamic radii determined by DLS measurements, as well as the particle size measured by SEM. Figure 1 shows the SEM micrographs of the samples. The data in Table 1 suggest that aggregation of particles in aqueous suspension was quite limited.

Cubic hematites were synthesized by gel-sol procedures with chloride as shape controller. The low- and medium-size particles (C1 and C2, with diameters of 250 and 990 nm, respectively) were obtained without the akaganeite washing step (second method), adopting a single heat treatment and temperatures of 120°C and 50°C for C1 and C2, respectively. The larger particles (C3, 1480 nm) were synthesized following the gel-sol procedure through the akaganeite washing step (first method). The concentration of chloride ions, used as shape controllers in the final heat treatment, was 1 M for C1 and C2, and 0.3 M for C3.

Spherical particles with low diameter (150 nm, sample S1) were obtained through the catalytic phase-transformation procedure (third method) with 0.5 M $FeCl_3$ (chloride was used as shape controller). Sample S2 (560 nm) was obtained via gel-sol at 90°C (second method), using nitrilotriacetate as shape controller. Finally, large ovoidal hematite particles (sample O1, 1690 nm) were obtained *via* gel-sol with the akaganeite washing step (first method), using 0.3 M nitrilotriacetate.

Figure 2 shows the XRD patterns of the obtained hematite particles. Each sample gave signals related to the α-Fe_2O_3 phase, thereby confirming that hematite was actually present. In the case of S1, the use of trace Fe^{II} in the synthetic route may be responsible for the detection of some additional peaks as impurities. The relevant XRD spectrum showed in fact signals related to magnetite ($Fe^{II}Fe^{III}{}_2O_4$) and maghemite (γ-$Fe^{III}{}_2O_3$). In contrast, the other samples only had signals related to hematite (α-$Fe^{III}{}_2O_3$).

The porosities of the synthesized hematite materials were investigated by means of BET surface area and DFT model, applied to N_2 adsorption/desorption isotherms carried out at 77 K. The results are summarized in Table 2, while the experimental BET curves are reported in Figure SM2 in the SM. All the obtained isotherms are of the IV type (IUPAC classification), which applies to mesoporous and macroporous systems.

Pseudo-cubic systems had low BET surface areas, with absence of microporosity and a DFT total volume calculated in the range of 0.01-0.04 $cm^3\ g^{-1}$ (slit pore shape). The measured porosity was probably due to inter-particle voids. S1 and O1 showed the highest BET surface areas among the studied samples (73 and 53 $m^2\ g^{-1}$, respectively), together with the highest DFT pore volumes (0.15 and 0.05 $cm^3\ g^{-1}$, respectively). Similar results were obtained by using the BJH method. In this case, it was not possible to exclude an intrinsic inter-particle porosity. Pseudo-cubic samples were less porous than the spherical ones. This phenomenon could be attributed to the different aggregation packing induced by the different geometry of the systems.

An interesting issue is that the surface areas were not inversely correlated with particle diameters: within cubic hematites the middle-sized sample (C2) had the largest surface area, while in the case of spherical/ovoidal ones the corresponding sample (S2) had the lowest area. SEM micrographs (Figure 1) suggest that particles had smooth surfaces, thus the unexpected BET trend might be due to particle aggregation. This issue could be consistent with porosity measures, which suggest the occurrence of inter-particle voids.

Figure 3 reports the extinction spectra of the cubic (3A) and spherical/ovoidal (3B) hematite samples, which are the result of the contributions of both absorption and scattering. Because hematite does not absorb radiation above 520 nm [46,47], the signals above that wavelength would be accounted for by scattering only. The spectra suggest that scattering of radiation is most important for the smallest particles (C1, S1). Although the assessment of the scattering is easy above 520 nm but much less straightforward below that wavelength, it is highly likely that the smallest particles also show important radiation scattering in the UV region.

3.2. Hematite photoactivity in photo-Fenton reactions

Preliminary experiments were carried out to assess the importance of H_2O_2, hematite and irradiation for phenol degradation. Insignificant degradation was observed upon irradiation of phenol and hematite alone, without H_2O_2, as well as in the presence of phenol, hematite and H_2O_2 in the dark. The dark experiments also ruled out a significant adsorption of phenol onto hematite. The direct photolysis of phenol and the degradation of phenol by irradiated H_2O_2 (irradiation without hematite in both cases) were negligible as well. Therefore, to achieve significant phenol degradation under the studied conditions, the contemporary presence of hematite, H_2O_2 and irradiation was required. The results of the preliminary experiments can be rationalized as follows:

(i) Phenol adsorption on hematite is at most very limited, which is reasonable considering the high phenol affinity for water. This issue does not rule out the possibility that degradation involves reactive species formed at the oxide surface [48], but one should also consider the alternative possibility that the reaction takes place in the solution bulk.

(ii) The lack of phenol degradation by hematite + H_2O_2 in the dark suggests that Fe^{III} on the oxide surface is much less reactive towards H_2O_2 compared to dissolved Fe^{III} species. This finding is consistent with the low (dark) Fenton reactivity reported for mineral surfaces containing Fe^{III} [49].

(iii) Irradiated hematite alone is unable to cause significant degradation of phenol. There is evidence that α-Fe_2O_3 under irradiation can induce charge-transfer reactions that are, however, considerably more effective towards inorganic ions compared to phenolic compounds [50]. The ability of inorganic ions (such as nitrite) to act as electron shuttles and favor the photodegradation of phenols by hematite (through the generation of reactive radical species, e.g. $^{\bullet}NO_2$) [31,50] suggests that the direct (shuttle-free) process is prevented by kinetic rather than by thermodynamic issues.

(iv) The negligible degradation of phenol by H_2O_2 alone under irradiation (without hematite) is most likely accounted for by the limited absorption by H_2O_2 of the radiation emitted by the lamp [51].

All of the above issues suggest that the degradation of phenol by hematite requires photo-Fenton conditions. First of all, the optimal pH for the heterogeneous photo-Fenton system was investigated. Using sample C2, 0.1 mM phenol + 1 mM H_2O_2 + 200 mg L^{-1} hematite were irradiated in the pH interval 2-5, adjusted with $HClO_4$. The variation of pH during irradiation was very limited and could be neglected. Figure 4 shows that low degradation of phenol was observed at pH 2 and 5 at

the adopted irradiation time scale (up to 4 h). In contrast, at pH 3 and 4 the degradation was slow in the first 2 h and then accelerated to produce complete phenol disappearance in less than 4 h. Such a trend (initially slow reaction followed by a considerable acceleration) can be due to two phenomena (in alternative, or even operational at the same time): *(i)* the reaction involves dissolved Fe species, and time is required for Fe to get dissolved and to reach a sufficiently high concentration in solution to trigger the degradation; *(ii)* the transformation intermediates of phenol (*e.g.* catechol and hydroquinone, which need time to accumulate) favor the reduction of Fe^{III} (either dissolved or on the oxide surface) to Fe^{II}. The latter undergoes much faster reaction with H_2O_2 compared to Fe^{III}, which enhances the Fenton degradation of phenol [52,53]. Coherently, transformation intermediates were detected upon phenol degradation at pH 3 and especially 4. Their levels were 1,4-benzoquinone > catechol > hydroquinone, with a cumulated concentration that was maximal at 2-3 h irradiation and did not exceed 0.025 mM.

Some of the detected intermediates, and in particular catechol and hydroquinone, could be able to enhance the formation of $^{\bullet}OH$ and other oxidizing species by favoring the reductive dissolution of hematite to produce Fe^{II}, which reacts in the Fenton process (reaction 2) [27,33,54]. However, the same intermediates could also act as scavengers of the photogenerated reactive species, which could inhibit the degradation of phenol. In the present case the addition of 0.01-0.02 mM levels of catechol or hydroquinone before irradiation did not modify significantly the degradation of phenol, suggesting either a compensation of the two phenomena, or a too low concentration of the photoproduced intermediates for a measurable effect to be detected.

The optimal pH value for the homogeneous Fenton process is usually around 3 [55-57]. The most likely reasons are the decrease of $^{\bullet}OH$ *vs*. ferryl production at higher pH (FeO^{2+} is less reactive than the hydroxyl radical) and, at pH ≠ 3 (either higher or lower), the slow reduction of the Fe^{III} species formed in reaction (2). The latter issue is accounted for by the fact that $FeOH^{2+}$, which prevails at pH ~ 3, is the Fe^{III} species undergoing the easiest reduction to Fe^{II} [58]:

$$FeOH^{2+} + H_2O_2 \rightarrow Fe^{2+} + HO_2^{\bullet} + H_2O \qquad (3)$$

$$FeOH^{2+} + HO_2^{\bullet} \rightarrow Fe^{2+} + O_2 + H_2O \qquad (4)$$

Under heterogeneous conditions, in the presence of α-Fe_2O_3 under irradiation, reactions (3,4) are probably of lesser importance because the key Fe^{2+} source is reaction (1). Moreover, the speciation of Fe^{III} might be less pivotal because most of it would be present as α-Fe_2O_3. A less important role played by Fe^{III} recycling to Fe^{2+} (reactions 3,4) might explain why, in the presence of hematite, the reaction did not lose efficiency when increasing the pH from 3 to 4.

The results reported in Figure 4 suggest that phenol transformation was practically the same at pH 3 and 4. Subsequent experiments were carried out at pH 4, which is preferable in practical applications because it saves reactants for pH adjustment.

Figure 5 reports the degradation of phenol in the presence of cubic (Figure 5a) and of spherical/ovoidal hematite samples (Figure 5b). In the latter case the middle-sized particles (S2, 580

nm) proved to be the most photoactive ones. This finding might look surprising when considering that S2 was the spherical/ovoidal sample with the lowest surface area (Table 2). However, a limited to negligible effect of particle size and surface area in heterogeneous photo-Fenton processes has already been observed in the case of magnetite [27], presumably because the process also depends on other issues such as iron dissolution. Moreover, as far as the measured BET surface area is concerned, the observed differences among the studied samples were possibly due to aggregation in the solid phase (inter-particle voids). Such an aggregation is likely lost in the aqueous suspensions, as suggested by the laser light scattering data reported in Table 1.

In the case of the cubic samples, the small-sized particles (C1, 250 nm) had the lowest activity. This issue might apparently be consistent with their very low surface area (9 m^2 g^{-1}, the lowest among the studied samples). However, caveats concerning the application of solid-phase BET measurements (where particle aggregation was probably important) to the suspension properties (where no evidence of aggregation was found) have already been reported. On the other hand, the largest cubic particles (C3, 1480 nm) were more active than the middle-sized ones (C2, 990 nm).

The quite (and somewhat unexpected) low photoactivity of the small hematite particles (C1, S1) could be accounted for by their elevated scattering of radiation, as suggested by the extinction spectra reported in Figure 3. Indeed, radiation scattering by semiconductor suspensions is able to interfere with absorption and to limit the rate of photocatalytic reactions [48]. In contrast, there could be some relationship between the photoactivity toward phenol degradation and the amount of dissolved Fe in solution. Figure 6 reports the trend of total dissolved Fe upon irradiation of the photoactive samples C3, C2 and S2, showing that the Fe levels were in the tens μg L^{-1} range. For the other hematite samples under irradiation, total dissolved Fe was detectable but it was below the quantification limit of the analytical method (*i.e.* < 10 μg Fe L^{-1}). Note that dissolved Fe mainly occurred as $Fe^{III}_{(aq)}$ in all the samples, due to the presence of H_2O_2 at acidic pH (the $Fe^{II}_{(aq)}$ levels would be kept low by reaction (2)).

The importance of dissolved Fe in the studied photo-Fenton process was further highlighted by additional control experiments. By irradiating $Fe(ClO_4)_3$ at tens μg Fe L^{-1} levels in the presence of 1 mM H_2O_2 at pH 4, the degradation kinetics of phenol was comparable to that observed in the presence of hematite (see Figure 5b). This issue suggests that an important fraction of phenol degradation would take place in the dissolved phase.

4. Conclusions

Hematite samples with controlled size and morphology were obtained by introducing variants in key points of the reported synthesis techniques. Cubic, spherical and ovoidal particles differed for both size and surface area but, in the present case, surface area measurements might not be a suitable indicator of the actual behavior of the suspended particles. Indeed, BET measurements suggested that particle aggregation in the solid phase might be important, while no evidence of

aggregation in aqueous suspension could be obtained by comparison between SEM measurements (solid phase) and DLS data (suspended particles in water).

One might expect smaller particles to be more photoactive, due to a larger contact interface between the solid and the solution. However, no obvious relationship could be obtained between the size of particles and their ability to induce phenol degradation under photo-Fenton conditions. The most likely reason is that the smallest particles (C1, S1) showed an important scattering of radiation, which would interfere with absorption and decrease their photoactivity. In contrast, middle-size or even large particles (S2, C2, C3) showed much smaller scattering and considerable photoactivity, which would be probably linked to a relatively large amount of dissolved Fe. In the studied systems, solid hematite would probably act as a Fe reservoir that would be released and/or activated under irradiation (Fe^{III} photoreduction to Fe^{2+}) for the Fenton process to take place in solution ($Fe^{2+} + H_2O_2$).

As far as the level of dissolved Fe is concerned, there would still be wide margins to increase it because the concentration of leached Fe for all the studied samples was in the μg L^{-1} range. This is safely below the mg L^{-1} limits for wastewater. Similar degradation results as for hematite could be obtained by using Fe(III) salts in the same concentration range (tens μg Fe L^{-1}): in practical applications, the choice between the two approaches (dissolved Fe(III) or hematite) could depend on the cost comparison between the use of a salt (to be discharged with wastewater) and the recovery of hematite from the aqueous suspension.

Acknowledgments

LD is kindly grateful to Rockwood Italia S.p.A., Divisione Silo, for the financial support to his PhD.

References

[1] S. D. Richardson, T. A. Ternes, Water Analysis: Emerging Contaminants and Current Issues, Anal. Chem. 86 (2014) 2813-2848

[2] E. M. Ferguson, M. Allinson, G. Allinson, S. E. Swearer, K. L. Hassell, Fluctuations in natural and synthetic estrogen concentrations in a tidal estuary in south-eastern Australia, Wat. Res. 47 (2013) 1604-1615.

[3] G. H. Dai, J. Huang, W. W. Chen, B. Wang, G. Yu, S. B. Deng, Major pharmaceuticals and personal care products (PPCPs) in wastewater treatment plant and receiving water in Beijing, China, and associated ecological risks, Bull. Environ. Contam. Toxicol. 92 (2014) 655-661.

[4] S. K. Kim, J. K. Im, Y. M. Kang, S. Y. Jung, Y. L. Kho, K. D. Zoh, Wastewater treatment plants (WWTPs)-derived national discharge loads of perfluorinated compounds (PFCs), J. Haz. Mat. 201 (2012) 82-91.

[5] A. K. Sarmah, M. T. Meyer, A. B. A. Boxall, A global perspective on the use, sales, exposure pathways, occurrence, fate and effects of veterinary antibiotics (VAs) in the environment, Chemosphere 65 (2006) 725-759.
[6] J. Corcoran, M. J. Winter, C. R. Tyler, Pharmaceuticals in the aquatic environment: A critical review of the evidence for health effects in fish, Crit. Rev. Toxicol. 40 (2010) 287-304.
[7] J. O. Tijani, O. O. Fatoba, L. F. Petrik, A review of pharmaceuticals and endocrine-disrupting compounds: Sources, effects, removal, and detections, Wat. Air Soil Pollut. 224 (2013) 1770.
[8] K. Kummerer, The presence of pharmaceuticals in the environment due to human use - present knowledge and future challenges, J. Environ. Manag. 90 (2009) 2354-2366.
[9] J. Hollender, S. G. Zimmermann, S. Koepke, M. Krauss, C. S. McArdell, C. Ort, H. Singer, U. von Gunten, H. Siegrist, Elimination of organic micropollutants in a municipal wastewater treatment plant upgraded with a full-scale post-ozonation followed by sand filtration, Environ. Sci. Technol. 43 (2009) 7862-7869.
[10] P. Verlicchi, S. Cattaneo, F. Marciano, L. Masotti, G. Vecchiato, C. Zaffaroni. Efficacy and reliability of upgraded industrial treatment plant at Porto Marghera, near Venice, Italy, in removing nutrients and dangerous micropollutants from petrochemical wastewaters, Wat. Environ. Res. 83 (2011) 739-749.
[11] M. Klavarioti, D. Mantzavinos, D. Kassinos, Removal of residual pharmaceuticals from aqueous systems by advanced oxidation processes, Environ. Intern. 35 (2009) 402-417.
[12] J. L. Wang, L. J. Xu, Advanced oxidation processes for wastewater treatment: Formation of hydroxyl radical and application, Crit. Rev. Environ. Sci. Technol. 42 (2012) 251-325.
[13] M. Petkovšek, M. Zupanc, M. Dular, T. Kosjek, E. Heath, B. Kompare, B. Širok, Rotation generator of hydrodynamic cavitation for water treatment, Sep. Purif. Technol. 118 (2013) 415-423.
[14] C. von Sonntag, The basics of oxidants in water treatment. Part A: OH radical reactions, Wat. Sci. Technol. 55 (2007) 19-23.
[15] M. A. Rauf, S. S. Ashraf, Radiation induced degradation of dyes-An overview, J. Haz. Mat. 166 (2009) 6-16.
[16] L. Prieto-Rodriguez, D. Spasiano, I. Oller, I. Fernandez-Calderero, A. Aguera, S. Malato, Solar photo-Fenton optimization for the treatment of MWTP effluents containing emerging contaminants, Catal. Today 209 (2013) 188-194.
[17] N. Klamerth, S. Malato, A. Aguera, A. Fernanzed-Alba, Photo-Fenton and modified photo-Fenton at neutral pH for the treatment of emerging contaminants in wastewater treatment plant effluents: A comparison, Wat. Res. 47 (2013) 833-840.
[18] S. M. Kumar, Degradation and mineralization, of organic contaminants by Fenton and photo-Fenton processes: Review of mechanisms and effects of organic and inorganic additives, Res. J. Chem. Environ. 15 (2011) 96-112.

460 [19] J. I. Nieto-Juarez, T. Kohn, Virus removal and inactivation by iron (hydr)oxide-mediated
461 Fenton-like processes under sunlight and in the dark, Photochem. Photobiol. Sci. 12 (2013)
462 1596-1605.
463 [20] N. Bataineh, O. Pestovsky, A. Bakac, pH-induced mechanistic changeover from hydroxyl
464 radicals to iron(IV) in the Fenton reaction, Chem. Sci. 3 (2012) 1594-1599.
465 [21] C. Minero, M. Lucchiari, V. Maurino, D. Vione, A quantitative assessment of the production
466 of (OH)-O-center dot and additional oxidants in the dark Fenton reaction: Fenton degradation
467 of aromatic amines, RSC Adv. 3 (2013) 26443-26450.
468 [22] J. Gomis, R. F. Vercher, A. M. Amat, D. O. Martire, M. C. Gonzalez, A. B. Prevot, E.
469 Montoneri, A. Arques, L. Carlos, Application of soluble bio-organic substances (SBO) as
470 photocatalysts for wastewater treatment: Sensitizing effect and photo-Fenton-like process,
471 Catal. Today 209 (2013) 176-180.
472 [23] B. Iurascu, I. Siminiceanu, D. Vione, M. A. Vicente, A. Gil, Phenol degradation in water
473 through a heterogeneous photo-Fenton process catalyzed by Fe-treated laponite, Wat. Res. 43
474 (2009) 1313-1322.
475 [24] M. Muruganandham, R.P.S. Suri, M. Sillanpaa, J. J. Wu, B. Ahmmad, S. Balachandran, M.
476 Swaminathan, Recent developments in heterogeneous catalyzed environmental remediation
477 processes, J. Nanosci. Nanotechnol. 14 (2014) 1898-1910.
478 [25] J. Herney-Ramirez, M. A. Vicente, L. M. Madeira, Heterogeneous photo-Fenton oxidation
479 with pillared clay-based catalysts for wastewater treatment: A review, Appl. Catal. B:
480 Environ. 98 (2010) 10-26.
481 [26] E. G. Garrido-Ramirez, B. K. G. Theng, M. L. Mora, Clays and oxide minerals as catalysts and
482 nanocatalysts in Fenton-like reactions - A review, Appl. Clay Sci. 47 (2010) 182-192.
483 [27] M. Minella, G. Marchetti, E. De Laurentiis, M. Malandrino, V. Maurino, C. Minero, D. Vione,
484 K. Hanna, Photo-Fenton oxidation of phenol with magnetite as iron source, Appl. Catal. B:
485 Environ. 154-155 (2014) 102-109.
486 [28] E. M. Rodriguez, G. Fernandez, P. M. Alvarez, R. Hernandez, F. J. Beltran, Photocatalytic
487 degradation of organics in water in the presence of iron oxides: Effects of pH and light source,
488 Appl. Catal. B: Environ. 102 (2011) 572-583.
489 [29] E. M. Rodriguez, G. Fernandez, N. Klamerth, M. I. Maldonado, P. M. Alvarez, S. Malato,
490 Efficiency of different solar advanced oxidation processes on the oxidation of bisphenol A in
491 water, Appl. Catal. B: Environ. 95 (2010) 228-237.
492 [30] P. Basnet, G. K. Larsen, R. P. Jadeja, Y. C. Hung, Y. P. Zhao, alpha-Fe_2O_3 Nanocolumns and
493 nanorods fabricated by electron beam evaporation for visible light photocatalytic and
494 antimicrobial applications, ACS Appl. Mater. Interf. 5 (2013) 2085-2095.
495 [31] D. Vione, V. Maurino, C. Minero, D. Borghesi, M. Lucchiari, E. Pelizzetti, New processes in
496 the environmental chemistry of nitrite. 2. The role of hydrogen peroxide, Environ. Sci.
497 Technol. 37 (2003) 4635-4641.

[32] D. A. Wheeler, G. M. Wang, Y. C. Ling, Y. Li, J. Z. Zhang, Nanostructured hematite: synthesis, characterization, charge carrier dynamics, and photoelectrochemical properties, Energy Environ. Sci. 5 (2012) 6682-6702.

[33] R. M. Cornell, U. Schwertmann, The iron oxides: structure, properties, reactions, occurrences and uses, Wiley-VCH, 2003.

[34] X. L. Hu, J. C. Yu, Continuous aspect-ratio tuning and fine shape control of monodisperse alpha-Fe_2O_3 nanocrystals by a programmed microwave-hydrothermal method, Adv. Function. Mater. 18 (2008) 880-887.

[35] I. Magario, F. S. García Einschlag, E. H. Rueda, J. Zygadlo, M.L. Ferreira, Mechanisms of radical generation in the removal of phenol derivatives and pigments using different Fe-based catalytic systems, J. Mol. Catal. A: Chem. 352 (2012) 1-20.

[36] S. X. Zhang, X. L. Zhao, H. Y. Niu, Y. Shi, Y. Q. Cai, G. B. Jiang, Superparamagnetic Fe_3O_4 nanoparticles as catalysts for the catalytic oxidation of phenolic and aniline compounds, J. Haz. Mat. 167 (2009) 560-566.

[37] F. Tisa, A. A. A. Raman, W. M. A. W. Daud, Applicability of fluidized bed reactor in recalcitrant compound degradation through advanced oxidation processes: A review, J. Environ. Manag. 146 (2014) 260-275.

[38] T. Sugimoto, Monodispersed Particles, Elsevier, Amsterdam, 2001.

[39] H. Itoh, T. Sugimoto, Systematic control of size, shape, structure, and magnetic properties of uniform magnetite and maghemite particles, J. Colloid Interface Sci. 265 (2003) 283-295.

[40] T. Sugimoto, Y. Wang, H. Itoh, A. Muramatsu, Systematic control of size, shape and internal structure of monodisperse alpha-Fe_2O_3 particles, Colloids Surface A: Physicochem. Eng. Aspects, 134 (1998) 265-279.

[41] H. Liu, Y. Wei, P. Li, Y. Zhang, Y. Sun, Catalytic synthesis of nanosized hematite particles in solution, Mater. Chem. Phys. 102 (2007) 1-6.

[42] S. Brunauer, P.H. Emmett, E. Teller, Adsorption of gases in multimolecular layers, J. Am. Chem. Soc. 60 (1938) 309-319.

[43] R. Nisticò, D. Scalarone, G. Magnacca, Preparation and physico-chemical characterization of large-mesopore silica thin films templated by block copolymers for membrane technology, Micropor. Mesopor. Mat. 190 (2014) 208-214.

[44] D.L. Ou, P.D. Chevalier, I.A. Mackinnon, K. Eguchi, R. Boisvert, K. Su, Preparation of microporous ORMOSILs by thermal degradation of organically modified siloxane resin, J. Sol-Gel. Sci. Technol. 26 (2003) 407-412.

[45] K. A. Riganakos, P. G. Veltsistas, Comparative spectrophotometric determination of the total iron content in various white and red Greek wines, Food Chem. 82 (2003) 637-643.

[46] J. K. Leland, A. J. Bard, Photochemistry of colloidal semiconducting iron oxide polymorphs, J. Phys. Chem. 91 (1987) 5076-5083.

[47] B. C. Faust, M. R. Hoffmann, D. W. Bahnemann, Photocatalytic oxidation of sulfur dioxide in aqueous suspensions of α-Fe_2O_3, J. Phys. Chem. 93 (1989) 6371-6381.

[48] C. Minero, D. Vione, A quantitative evalution of the photocatalytic performance of TiO_2 slurries, Appl. Catal. B: Environ. 67 (2006) 257-269.
[49] W. Y. Huang, M. Brigante, F. Wu, K. Hanna, G. Mailhot, Effect of ethylenediamine-N,N'-disuccinic acid on Fenton and photo-Fenton processes using goethite as an iron source: optimization of parameters for bisphenol A degradation, Environ. Sci. Pollut. Res. 20 (2013) 39-50.
[50] D. Vione, V. Maurino, C. Minero, E. Pelizzetti, Aqueous atmospheric chemistry: Formation of 2,4-dinitrophenol upon nitration of 2-nitrophenol and 4-nitrophenol in solution, Environ. Sci. Technol. 39 (2005) 7921-7931.
[51] B. J. Finlayson-Pitts, J. N. Pitts Jr., Chemistry of the Upper and Lower Atmosphere - Theory, Experiments, and Applications, Academic Press, San Diego, 2000.
[52] Y.X. Du, M.H. Zhou, L.C. Lei, Role of the intermediates in the degradation of phenolic compounds by Fenton-like process, J. Haz. Mat. 136 (2006) 859-865.
[53] X. L. Hao, M. H. Zhou, Q. Xin, L. C. Lei, Pulsed discharge plasma induced Fenton-like reactions for the enhancement of the degradation of 4-chlorophenol in water, Chemosphere 66 (2007) 2185-2192.
[54] H. Gulley-Stahl, P. A. Hogan, W. L. Schmidt, S. J. Wall, A. B. Buhrlage, H. A. Bullen, Surface complexation of catechol to metal oxides: An ATR-FTIR, adsorption, and dissolution study. Environ. Sci. Technol. 44 (2010) 4116-4121.
[55] P. P. Marcinowski, J. P. Bogacki, J. H. Naumczyk, Cosmetic wastewater treatment using the Fenton, Photo-Fenton and H_2O_2/UV processes, J. Environ. Sci. Health Part A-Toxic/Hazard. Subst. Environ. Eng. 49 (2014) 1531-1541.
[56] R. C. Martins, M. Nunes, L. M. Gando-Ferreira, R. M. Quinta-Ferreira, Nanofiltration and Fenton's process over iron shavings for surfactants removal, Environ. Technol. 35 (2014) 2380-2388.
[57] S. Y. Zhang, Y. Z. Han, L. Wang, Y. L. Chen, P. Y. Zhang, Treatment of hypersaline industrial wastewater from salicylaldehyde production by heterogeneous catalytic wet peroxide oxidation on commercial activated carbon, Chem. Eng. J. 252 (2014) 141-149.
[58] D. L. Sedlak, J. Hoigné, The role of copper and oxalate in the redox cycling of iron in atmospheric waters, Atmos. Environ. 27 (1993) 2173-2185.

568

569

570 **Table 1.** Particle size (edge length or diameter) and hydrodynamic radii (HR) of the synthesized
571 hematite particles.

572

Sample	Size, nm	HR, nm	Preparation method
C1	250	190	120°C, no akaganeite washing, 1 M Cl^- as shape controller
C2	990	460	50°C, no akaganeite washing, 1 M Cl^- as shape controller
C3	1480	480	Akaganeite washing, 0.3 M Cl^- as shape controller
S1	150	100	Catalytic phase transformation, 0.5 M $FeCl_3$, chloride as shape controller
S2	560	280	90°C, no akaganeite washing, nitrilotriacetate as shape controller
O1	1690	510	Akaganeite washing, nitrilotriacetate as shape controller

573

574

575

576

577

578

579 **Table 2.** BET specific surface areas and porosity details of hematite samples.

580

Sample	BET surface area ($m^2\ g^{-1}$)	DFT pore volume ($cm^3\ g^{-1}$)
C1	9	0.04
C2	26	0.03
C3	12	0.01
S1	73	0.15
S2	21	0.02
O1	53	0.05

581

582

583

Captions to the Figures

Figure 1. SEM micrographs of the synthesized hematite particles. Particle sizes are reported in Table 1.

Figure 2. X-Ray Diffraction patterns of the synthesized hematite samples.

Figure 3. Extinction spectra of the cubic (A) and spherical/ovoidal (B) hematite samples (loading of 100 mg L^{-1} α-Fe_2O_3.). Data are referred to an optical path length of 10 mm.

Figure 4. Phenol degradation as a function of pH. Initial conditions: 0.1 mM phenol, 1 mM H_2O_2, 200 mg L^{-1} hematite (C2) loading, UV irradiation.

Figure 5. Plot of phenol degradation in presence of cubic (a) and spherical/ovoidal (b) hematite samples at pH 4. Initial conditions: 0.1 mM phenol, 1 mM H_2O_2, 200 mg L^{-1} hematite loading, UV irradiation. The error bars represent the standard errors of duplicate experiments. Figure 5(b) also reports the results of experiments carried out upon irradiation of $Fe(ClO_4)_3$ at 10 and 50 μg Fe L^{-1}, under otherwise identical conditions as for the hematite runs but by replacing hematite with $Fe(ClO_4)_3$ as Fe compound.

Figure 6. Time trend of total dissolved Fe upon UV irradiation of 0.1 mM phenol, 1 mM H_2O_2 and 200 mg L^{-1} hematite (C2, C3 and S2) at pH 4. Total dissolved Fe was mainly in the form of Fe(III).

610 **Figure 1**

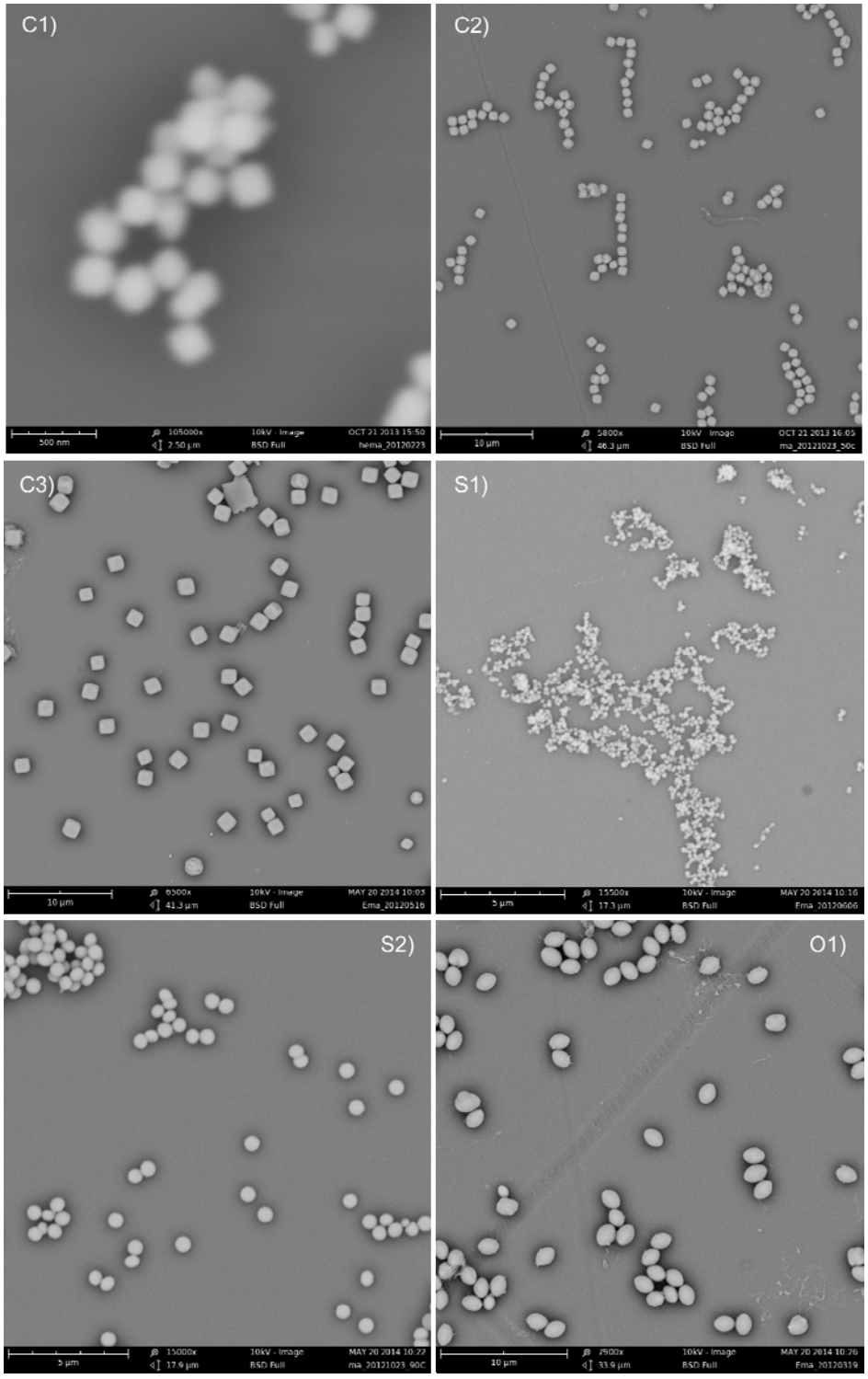

611
612

613 **Figure 2**

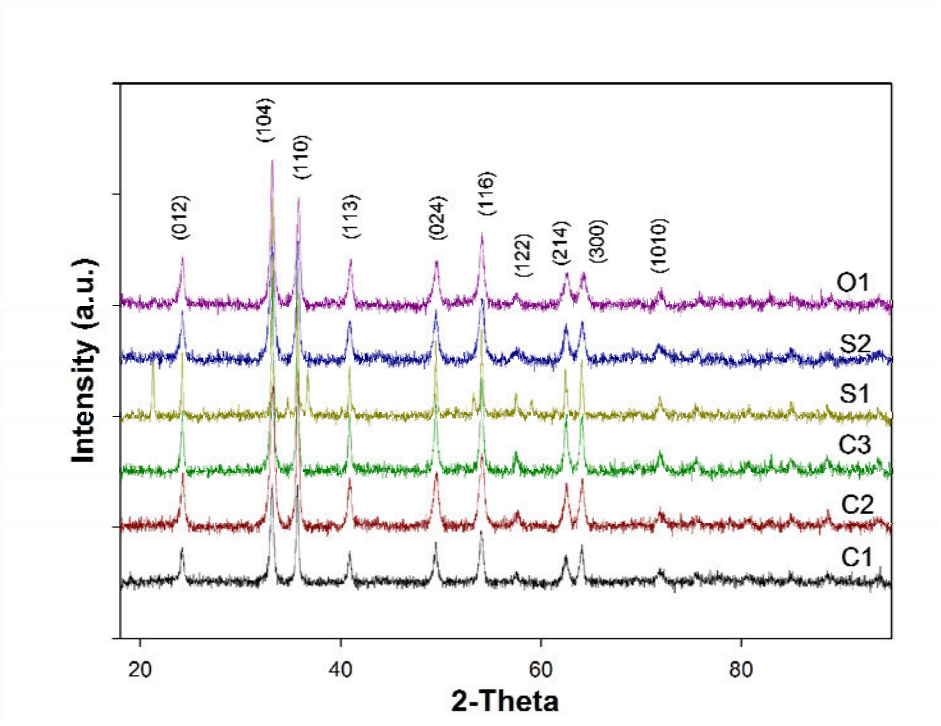

614
615

616 **Figure 3**

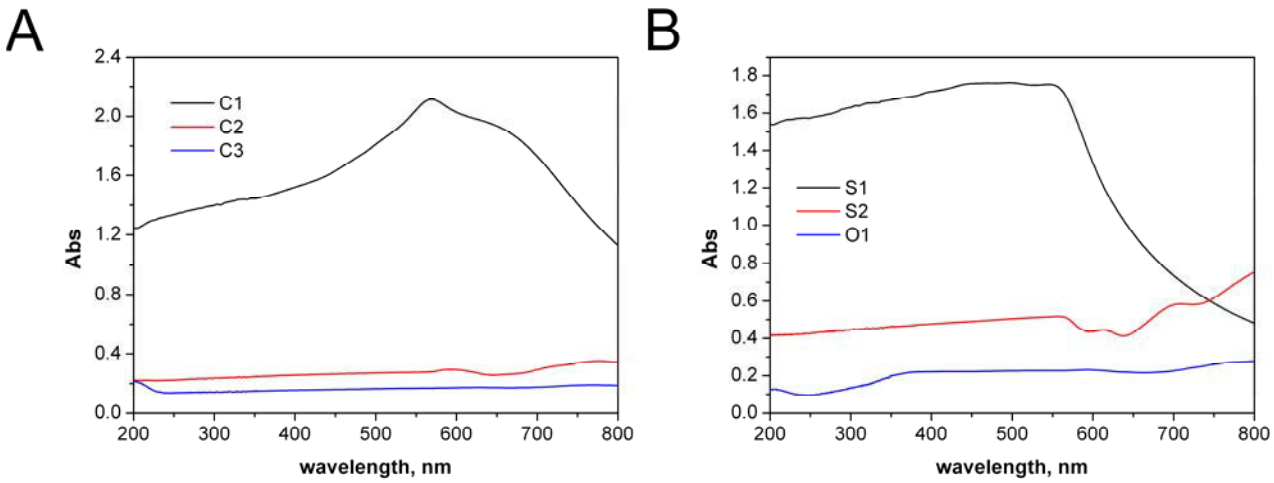

617
618

619 **Figure 4**

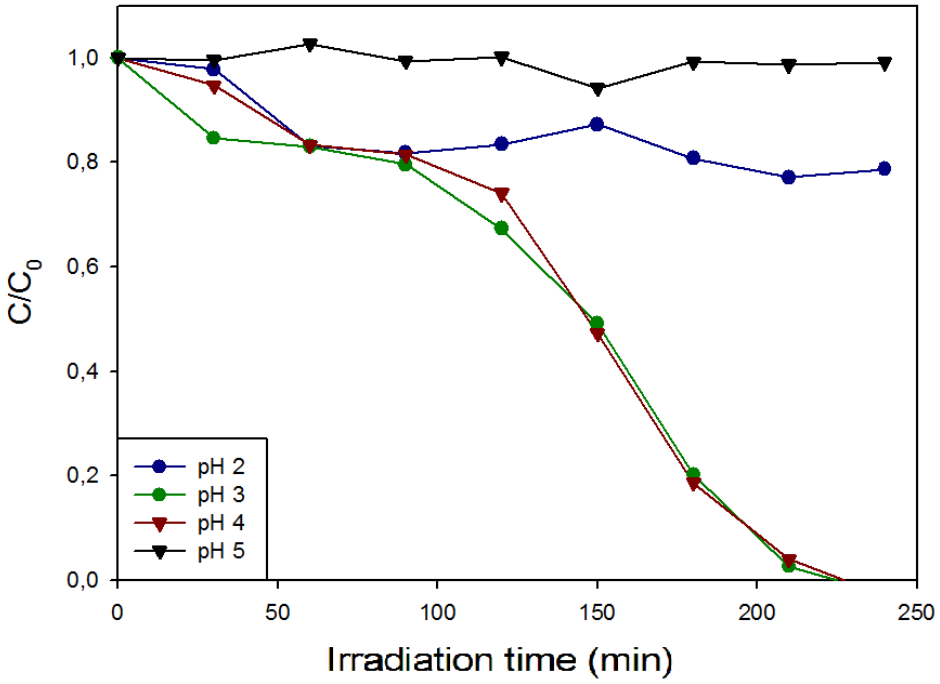

620
621

622 **Figure 5**

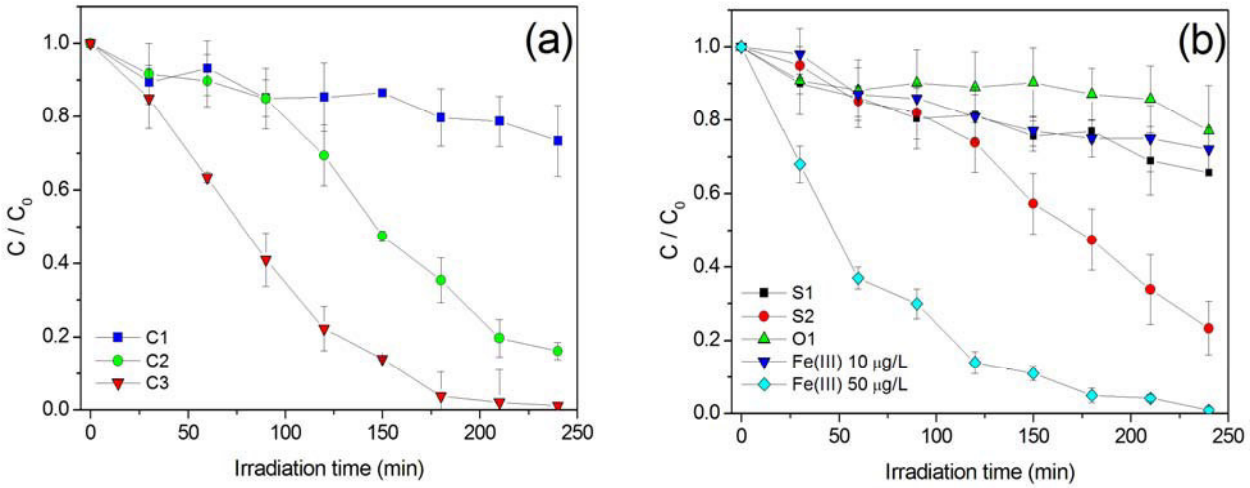

623
624

625 **Figure 6**

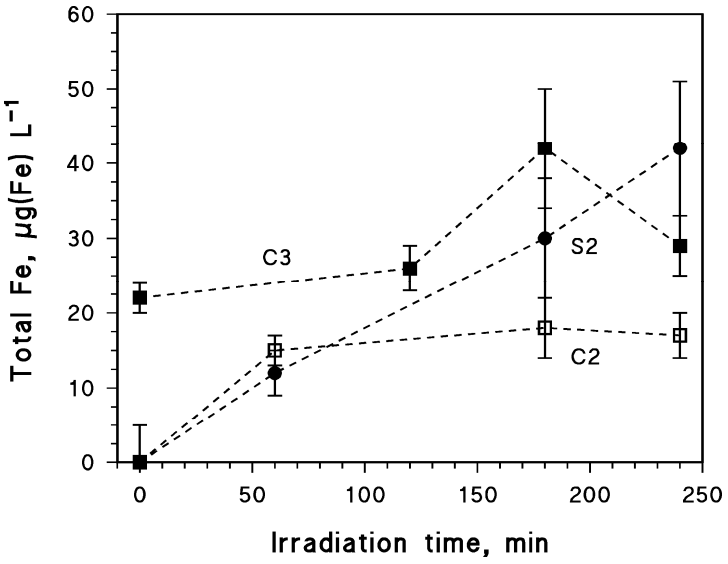

626

SUPPLEMENTARY MATERIAL

Heterogeneous photo-Fenton reaction in the presence of morphologically controlled hematite

Luca Demarchis, Marco Minella, Roberto Nisticò, Valter Maurino, Claudio Minero, Davide Vione*

Università di Torino, Dipartimento di Chimica, Via Pietro Giuria 5-7, 10125 Torino, Italy.

* Corresponding Author

E-mail: *davide.vione@unito.it*. Phone +39-011-6705296. Fax: +39-011-6705242.

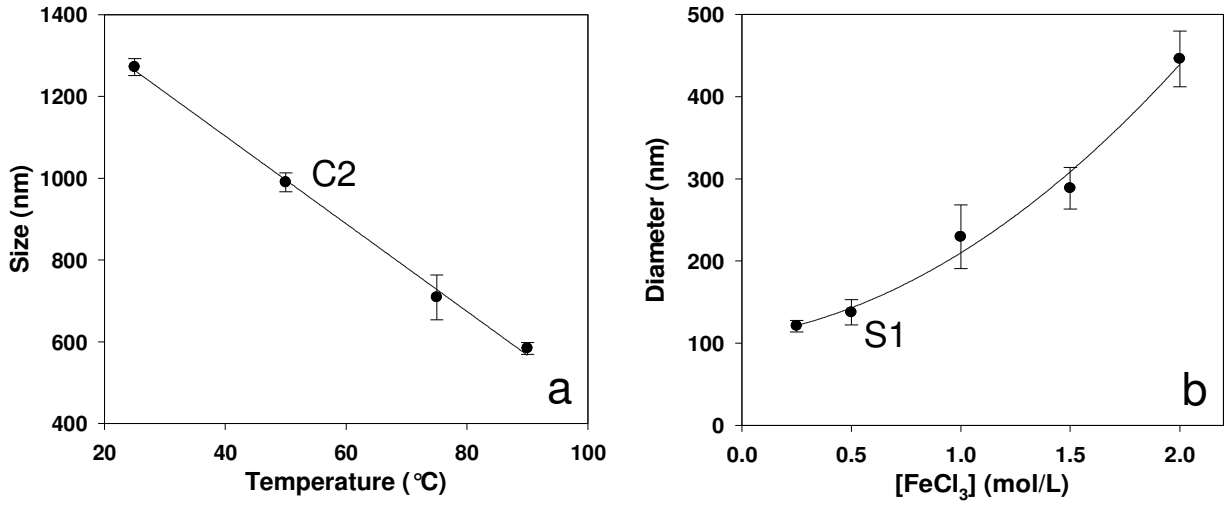

Figure SM1. (a) Size of hematite cubic particles (edge length) obtained via the gel-sol method, as a function of the initial temperature. Chloride was used as shape controller. Other conditions are described in the text. **(b)** Diameter of spherical hematite particles obtained with the catalytic phase-transformation method, as a function of $FeCl_3$ concentration. Other conditions are described in the text. Samples C2 and S1 are highlighted on the plots.

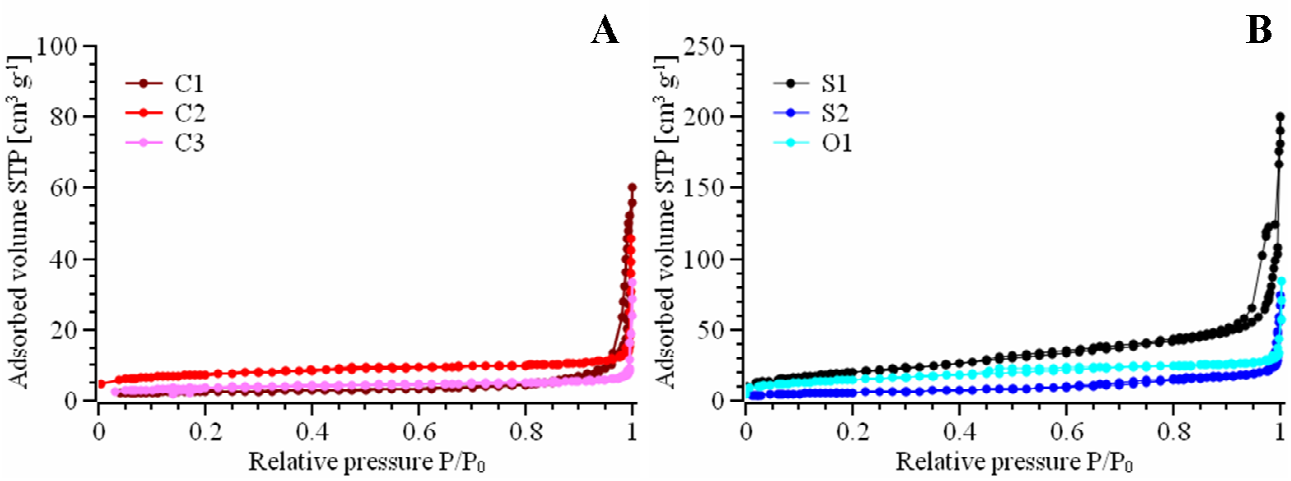

Figure SM2. N_2 adsorption/desorption isotherms at 77 K for (A) pseudo-cubic and (B) spherical/ovoidal hematite samples.